DOI: 10.1002/chem.200800801

Metal-Controlled Anion-Binding Tendencies of the Thiourea Unit of Thiosemicarbazones

Valeria Amendola,[a] Massimo Boiocchi,[b] Luigi Fabbrizzi,*[a] and Lorenzo Mosca[a]

Abstract: The terdentate ligand **3** (LH, 2-formylpyridine 4-thiosemicarbazone) forms with Fe^{II} and Ni^{II} 2:1 complexes of octahedral geometry of formula $[M^{II}(LH)_2]^{2+}$. X-ray diffraction studies have shown that in both complexes the thiourea moieties of the coordinated thiosemicarbazones are exposed to the outside and are prone to establish hydrogen-bonding bifurcate interactions with oxoanions. However, spectrophotometric studies in $CHCl_3$ solution have shown that only the poorly basic NO_3^- ion is able to form authentic hydrogen-bond complexes with thiourea subunits, whereas all the other investigated anions (CH_3COO^-, NO_2^-, F^-) induce deprotonation of the N-H fragment. The extreme enhancement of the thiourea acidity is based on the coordinative interaction of the sulphur atom with the metal, which stabilises the thiolate form, and it is much higher than that exerted by any other covalently linked electron-withdrawing substituent, for example, $-NO_2$.

Keywords: anions · charge transfer · hydrogen bonds · receptors · supramolecular chemistry

Introduction

Anion recognition by neutral H-bond donor receptors has become a challenging theme in supramolecular chemistry and represents an area of fervent research.[1] The most frequently used H-bond donating group is the N-H fragment from amides,[2] sulfonamides,[3] amines,[4] pyrroles,[5] ureas and thioureas.[6] A urea/thiourea subunit can donate two hydrogen bonds according to a bifurcate mode and is therefore an ideal receptor for anions that present two proximate oxygen atoms, for example, carboxylates and inorganic oxoanions. Hydrogen bonding can be considered as a more or less advanced proton transfer from the donor (the receptor) to the acceptor (the anion).[7] The more acidic the receptor, the more advanced the proton transfer and the stronger the receptor–anion interaction. It is for this reason that the rather acidic thiourea fragment (pK_A 21.1 in DMSO) establishes with oxoanions stronger interactions than the distinctly less acidic urea (pK_A 26.9 in DMSO).[8] In a limiting situation, urea- and thiourea-based receptors, made particularly acidic by covalently linked electron withdrawing substituents, may undergo deprotonation of one N-H fragment on interaction with strongly basic anions.[9] This is a rather common behaviour in the presence of an excess of fluoride, due to the formation of the particularly stable HF_2^- hydrogen bonding self-complex.[10] Also, the solvent plays a role in controlling N-H deprotonation. In particular, deprotonation and formation of the $[HA_2]^-$ self-complex are favoured by more polar media, which stabilise the negatively charged products. For instance, derivative **1** in a DMSO solution undergoes N-H deprotonation not only in presence of fluoride, but also on addition of excess acetate, with formation of the $[CH_3COOH\cdots CH_3COO]^-$ self-complex.[11] Quantitative aspects of anion induced N-H deprotonation of urea–thiourea derivatives have been clearly discussed in a recent article.[12]

[a] Dr. V. Amendola, Prof. L. Fabbrizzi, Dr. L. Mosca
Dipartimento di Chimica Generale, Università di Pavia
via Taramelli 12, 27100 Pavia (Italy)
Fax: (+39) 382-528544
E-mail: luigi.fabbrizzi@unipv.it

[b] Dr. M. Boiocchi
Centro Grandi Strumenti, Università di Pavia
via Bassi, 27100 Pavia (Italy)

Supporting information for this article is available on the WWW under http://dx.doi.org/10.1002/chem.200800801: Structures of the $[Fe^{II}(\mathbf{3})_2]^{2+}$ and $[Ni^{II}(\mathbf{3})_2]^{2+}$ complexes, supplementary spectrophotometric titrations and the colour photographs of the $CHCl_3$ solutions of the $[Fe^{II}(\mathbf{3})_2]^{2+}$ and $[Ni^{II}(\mathbf{3})_2]^{2+}$ complexes after the addition of 0, 1, and 2 equiv of base.

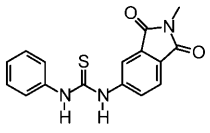

1

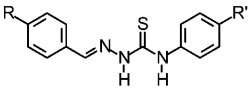

2

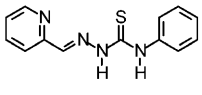

3 (LH)

We have recently investigated the interaction of a family of R-substituted-benzylideneamine-*N'*-(R[1]-substituted-phenyl)thioureas (**2**) with a variety of anions in MeCN solution.[13] The formation of genuine H-bond association complexes with CH_3COO^- and $H_2PO_4^-$ was observed, whereas F^- induced deprotonation. Other oxoanions (HSO_4^-, NO_2^-, NO_3^-) did not form any complex even with receptors equipped with powerful electron-withdrawing substituents (e.g. NO_2, CF_3).

We assumed that a transition-metal ion, conveniently coordinated to the benzylidene-thiourea framework, could act as a powerful electron-withdrawing substituent, thus enhancing the acidity of the thiourea fragment and hopefully inducing novel selectivity effects in anion recognition. Thus, we have prepared derivative **3**, in which the benzylidene phenyl ring of receptor **2** has been replaced by a pyridine ring. System **3** can behave as a terdentate ligand (LH) through an N_2S donor set (as indicated by arrows in the formula) and can give 1:2 complexes of formula $[M^{II}(LH)_2]^{2+}$ with metals prone to six-coordination and octahedral geometry, for example, Fe^{II}, Ni^{II}, as illustrated in Scheme 1.

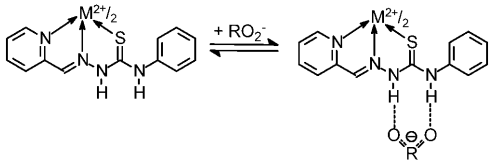

Scheme 1. Interaction of $[M^{II}(\mathbf{3})_2]^{2+}$ complexes (M = Fe, Ni) with oxoanions.

In principle, in the $[M^{II}(LH)_2]^{2+}$ metal complex, the two thiourea subunits can interact with two oxoanions RO_2^-, according to the equilibrium shown in Scheme 1 (constituted by two steps), to give eventually the genuine H-bond complex $[M^{II}(LH)_2(\cdots RO_2)_2]^{2+}$. Moreover, the role of the coordinated metal centre, as an electron-withdrawing group, on the polarization of thiourea N-H fragments has to be considered, which may lead to stepwise deprotonation.

We describe here an investigation on the interaction of octahedral complexes of type $[M^{II}(LH)_2]^{2+}$ (M = Fe, Ni) with anions in a $CHCl_3$ solution. It will be shown that most anions promote N-H deprotonation, according to two distinct steps, signalled by noticeable colour changes. Only the poorly basic nitrate ion is able to form stable and authentic hydrogen bonding complexes, still in a stepwise mode, with moderate colour modifications.

Results and Discussion

Anion affinity of thioureas in a $CHCl_3$ solution: The complexation equilibria of a variety of thiourea derivatives towards anions have been investigated in media of different polarity. On the other hand, it has been previously pointed out that the higher the solvent polarity, the more pronounced the tendency of the receptor to deprotonate in presence of basic anions. In this study, we have chosen as a solvent the poorly polar chloroform, with the aim of favouring the formation of genuine receptor–anion H-bond complexes. In order to assess anion binding tendencies of thiourea-based receptors in chloroform, we carried out preliminary investigations with the thiourea derivative **4**.

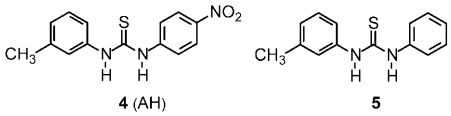

In **4**, a 4-nitrophenyl substituent has been appended to the thiourea unit in order i) to increase H-bond donating tendencies and ii) to provide a powerful chromogenic reporter for signalling anion binding. On the other hand, the methyl group in the *meta* position of the other phenyl substituent reduces the symmetry of the molecule, thus affording surprisingly high solubility in $CHCl_3$ (up to 0.1 M). Figure 1 shows the family of spectra recorded over the course of the titration of a solution of **4** in $CHCl_3$ with a standard solution of $[Bu_4N]CH_3COO$.

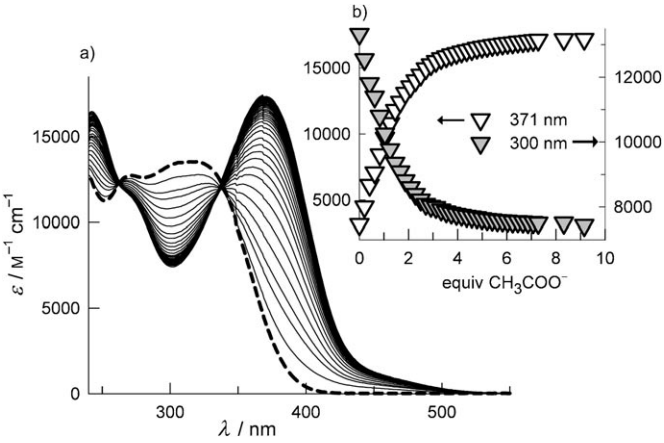

Figure 1. a) Spectra taken over the course of the titration of a 5.04×10^{-5} M solution of **4** in $CHCl_3$ with a solution 6.34×10^{-3} M of $[Bu_4N]CH_3COO$ in $CHCl_3$; -----: refers to the spectrum of receptor **4**, before anion addition; b) titration profiles at selected wavelengths: ▽, band centred at 300 nm, pertinent to the uncomplexed receptor **4** (AH), decreasing profile; ▽: band centred at 371 nm, pertinent to the hydrogen-bonding complex $[AH\cdots CH_3COO]^-$, increasing profile.

The receptor shows two overlapping bands, one centred at 270, the other at 315 nm. It is suggested that the two bands result from charge-transfer transitions to the nitrophenyl substituents, one from the tolyl subunit, the other from the thiourea subunit.

Upon acetate addition, the spectrum undergoes two major modifications: i) the intensity of the band at 270 nm undergoes a moderate decrease; ii) the band at 315 nm experiences a drastic red shift: in particular, a new band devel-

ops at 370 nm. It is suggested that the band at 315 nm originates from a charge-transfer transition from the thiourea subunit to the nitrobenzene subunit and that the urea–acetate interaction stabilises the excited state resulting from such a transition, thus inducing a significant bathochromic shift of the absorption band. The tolyl-to-nitrophenyl charge transfer is not perturbed by the thiourea–acetate interaction and the corresponding band, centred at 270 nm, does not undergo any red shift. Moreover, multi-wavelength treatment of titration data over the 250–550 nm range, by HyperQuad program,[14] indicated the formation of a receptor-anion complex of 1:1 stoichiometry, $[AH\cdots CH_3COO]^-$, according to Equilibrium (1):

$$AH + X^- \rightleftharpoons [AH\cdots X]^- \quad (1)$$

with a $\log K = 4.44 \pm 0.03$. It has to be noted that semiempirical studies, using PM3 method, suggested that the uncomplexed receptor **4** should exist in the *trans* conformation illustrated by formula **6**. Therefore, anion binding should induce a geometrical rearrangement of **4**, from the *trans* conformation **6** to the *cis* conformation **7**, required for establishing bifurcate hydrogen-bonding interaction with acetate and pictorially illustrated in Scheme 2.

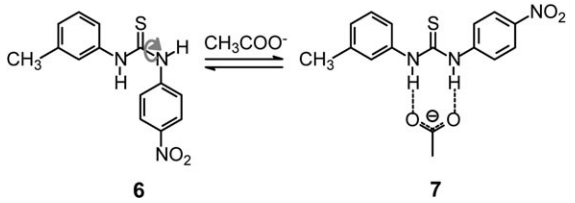

Scheme 2. Formation of the H-bond complex **7** induces a conformational rearrangement of receptor **6**, from the stable *trans* arrangement (the nitrophenyl substituent is *trans* with respect to the thiourea sulphur atom) to the *cis* arrangement, suitable for bifurcate hydrogen bonding interaction with the acetate ion.

A similar behaviour was observed on spectrophotometric titration of **4** with a variety of oxoanions: $H_2PO_4^-$, HSO_4^-, NO_2^-, NO_3^-. In particular, a red shift of the band at 315 nm was observed on anion addition and titration data could be interpreted on assuming the formation of a 1:1 receptor–anion complex, $[AH\cdots X]^-$, according to Equation (1). Limiting spectra obtained on addition of a large anion excess are shown in Figure 2a. log*K* values for Equation (1) involving the investigated anions are reported in Table 1.

The stability of the $[AH\cdots X]^-$ complex decreases along the series $CH_3COO^- > H_2PO_4^- > HSO_4^- > NO_2^- > NO_3^-$, which reflects the decreasing basicity of the anion, a behaviour typically observed in the interaction of urea- and thiourea-based receptors with anions. Hydrogen bonding has been defined as a more or less advanced (and "frozen") proton transfer from the donor (the receptor) to the acceptor (the anion).[7] The more basic the anion, the more advanced the proton transfer, the stronger the H-bond interaction. Quite interestingly, also the magnitude of the red shift decreases according to the same sequence: $CH_3COO^- > H_2PO_4^- > HSO_4^- > NO_2^- > NO_3^-$. In particular, a rough linear relationship exists between log*K* and the wavelength of the absorption band of the $[AH\cdots X]^-$ complex (see Figure 2b). Such a correlation is not surprising, if one considers that the interaction with the oxoanion stabilizes the charge transfer excited state of the receptor: the stronger anion basicity, the more pronounced the stabilization of the excited state, the lower the energy of the optical transition(s). In any case, it is demonstrated once again that the stability of the H-bond complexes does not reflect any geometrical complementarity between the N-H fragments of the urea/thiourea subunit and two consecutive oxygen atoms of the anion, but simply depends upon the basic tendencies of the oxoanion.

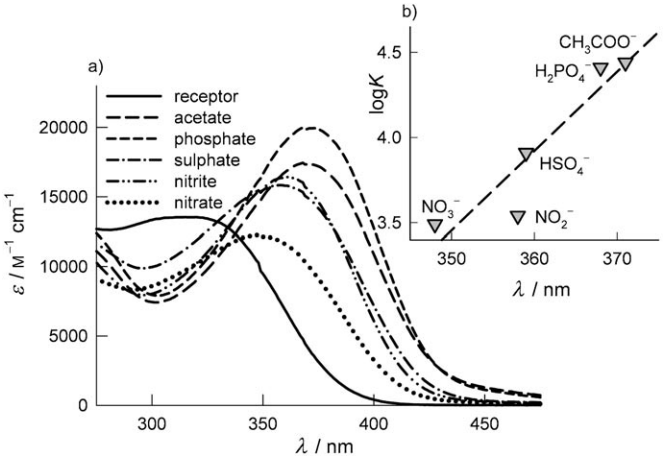

Figure 2. a) Spectra obtained on addition of a large anion excess to a solution of **4** in $CHCl_3$; b) plot of the log*K* values for the receptor–anion equilibrium vs. the wavelength of the absorption band of the pertinent receptor-anion complex, as taken from limiting spectra in Figure 2a.

Table 1. log*K* values for the formation of H-bond complexes in $CHCl_3$ solution, at 25 °C, according to the equilibrium: $AH + X^- \rightleftarrows [AH\cdots X]^-$. $\log K_2$ for F^- refers to the equilibrium: $[AH\cdots F]^- + F^- \rightleftarrows A^- + HF_2^-$.

Anion	**4** (AH)	**5**
CH_3COO^-	4.44 ± 0.03	2.7 ± 0.1
NO_2^-	3.54 ± 0.01	–
F^-	$\log K_1 = 5.31 \pm 0.01$; $\log K_2 = 4.29 \pm 0.01$	2.74 ± 0.01
HSO_4^-	3.91 ± 0.01	–
$H_2PO_4^-$	4.41 ± 0.01	–
NO_3^-	3.49 ± 0.01	–

Halide ions showed a markedly different behaviour. In fact, addition of a large excess of tetraalkylammonium chloride, bromide and iodide salts to a $CHCl_3$ solution of **4** did not induce any spectral change, indicating no or very poor receptor–anion interaction. On the other hand, fluoride exhibited a rather intricate behaviour. Figure 3 displays the family of spectra taken over the course of the titration of a solution of **4** in $CHCl_3$ with a standard solution of $[Bu_4N]F\cdot 3H_2O$.

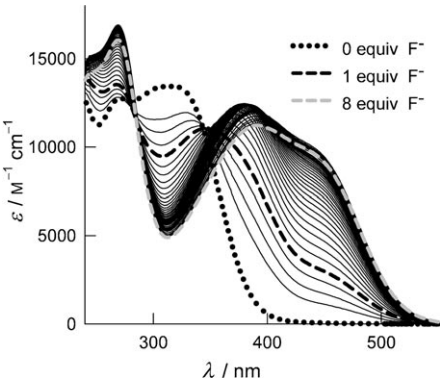

Figure 3. Spectra recorded over the course of the titration of a 5.08×10^{-5} M solution of **4** in $CHCl_3$ with a solution 5.14×10^{-3} M of $[Bu_4N]F\cdot3H_2O$ in $CHCl_3$. Spectra taken on solutions containing 0 equiv of fluoride (•••••), 1 equiv of fluoride (-----); 8 equiv of fluoride (- - - -) are indicated.

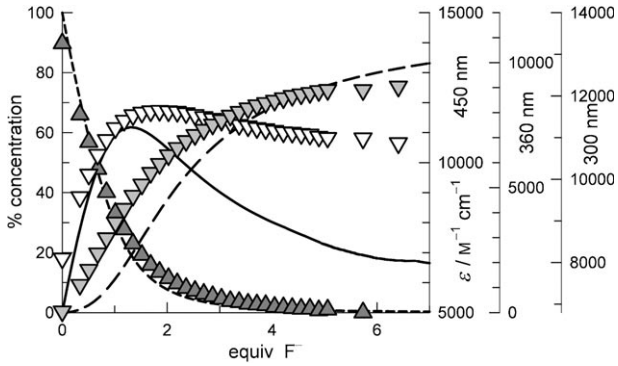

Figure 4. Lines (left vertical axis): concentration of the species which form over the course of the titration illustrated in Figure 4 (AH = **4**, -----). Symbols (right vertical axes): absorbance at selected wavelengths over the course of the titration; the band at 300 nm (▲) pertains to the uncomplexed receptor AH, the band at 360 nm (▽) to the H-bond complex $[AH\cdots F]^-$ (——), the band at 450 nm (▼) to the deprotonated form A^- (– – –).

Addition of fluoride first induces a moderate red shift of the band at 315 nm (thiourea-to-nitrophenyl charge-transfer transition), which indicates the formation of a genuine H-bond complex $[AH\cdots F]^-$, according to Equation (1). In Figure 3, the spectrum taken upon addition of 1 equiv of fluoride has been drawn as a black dashed line. However, on further anion addition, a more pronounced red shift of the absorption band is observed. Such a spectrum, drawn as a grey dashed line in Figure 3, clearly displays a two-transition nature. It is suggested that such a spectrum pertains to the deprotonated form of the receptor, A^-, which results from Equation (2)

$$[AH\cdots F]^- + F^- \rightleftharpoons A^- + [HF_2]^- \qquad (2)$$

Deprotonation of the N-H fragment of urea and thiourea derivatives on addition of excess fluoride has been observed for a variety of anion receptors and has to be ultimately ascribed to the high stability of the $[HF_2]^-$ self-complex;[7] in fact, *one* F^- is not an especially strong base, but *two* F^- are. Best fitting of titration data using the HyperQuad program was obtained on assuming the occurrence of stepwise Equilibria (1) and (2), to which the following values of K_1 and K_2 correspond: $\log K_1 = 5.31 \pm 0.01$, $\log K_2 = 4.29 \pm 0.02$.

Figure 4 reports the concentration profiles of the three species present at the equilibrium over the course of the titration: AH, $[AH\cdots F]^-$, A^-. It is observed that the H-bond complex, $[AH\cdots F]^-$, reaches its maximum concentration, about 60%, on addition of 1 equiv of fluoride. Interestingly, the absorbance at 360 nm, which refers to the maximum of the band drawn as a black dashed line in Figure 4, superimposes onto the ascending branch of the concentration profile of the H-bond complex $[AH\cdots F]^-$. Likewise, the absorbance at 450 nm, which refers to the higher wavelength component of the spectrum drawn as a grey dashed line in Figure 4, parallels the increase of the concentration profile of the deprotonated receptor A^-. It is also suggested (and corroborated by semi-empirical calculations) that on fluoride release and deprotonation, the receptor moves again to a *trans* conformation, as represented by structural formula **8** in Scheme 3.

It is suggested that form A^- is stabilised by the circumstance that the negative charge left on the thiourea nitrogen atom upon proton release can delocalize, through a π mechanism, onto the NO_2 fragment of the nitrophenyl substituent, as pictorially illustrated by the resonance formula **9** in Scheme 3. Notice that the excess of electronic charge on the NO_2 fragment increases the intensity of the dipole of *both* charge transfer transitions (at 270 and 315 nm in the neutral form AH), which are bathochromically shifted at 385 and 435 nm in the deprotonated form A^-.

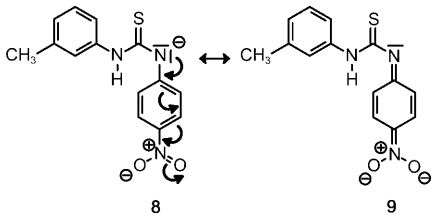

Scheme 3. Resonance representation of the deprotonated form of receptor **4**. The electronic charge left on the thiourea nitrogen atom following N-H deprotonation (limiting formula **8**) delocalizes onto the $-NO_2$ group of the nitrophenyl substituent, according to limiting formula 9.

The major role played by the nitrophenyl substituent in enhancing the acidity of the proximate N-H fragment has been further demonstrated by the behaviour of the thiourea derivative **5**, in which the $-NO_2$ group has been removed. Figure 5 displays the family of spectra recorded over the course of the titration of a solution of **5** in $CHCl_3$ with a standard solution of $[Bu_4N]F\cdot3H_2O$.

It is observed that even large excess addition of fluoride induces only a moderate shift of the charge transfer band of the receptor, which indicates the formation of a hydrogen-bonding complex of low thermodynamic stability. In particu-

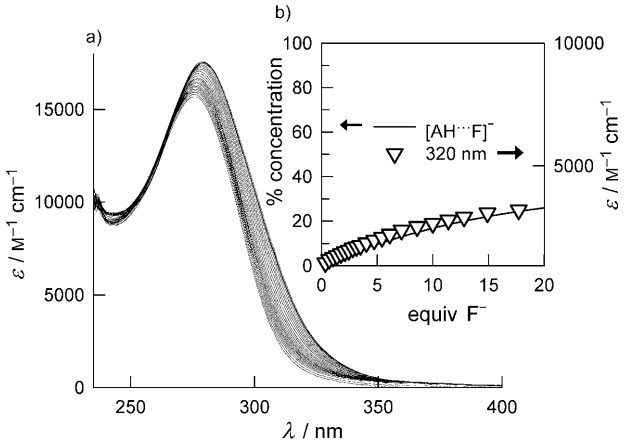

Figure 5. a) Spectra obtained over the course of the titration of a 4.79×10^{-5} M solution of **5** in $CHCl_3$ with a solution 5.04×10^{-3} M of $[Bu_4N]F\cdot3H_2O$ in $CHCl_3$; b) absorbance values at 320 nm (▽, ε right vertical axis) superimpose well on the concentration profile of the H-bond complex $[A\text{-}H\cdots F]^-$ (——, left vertical axis).

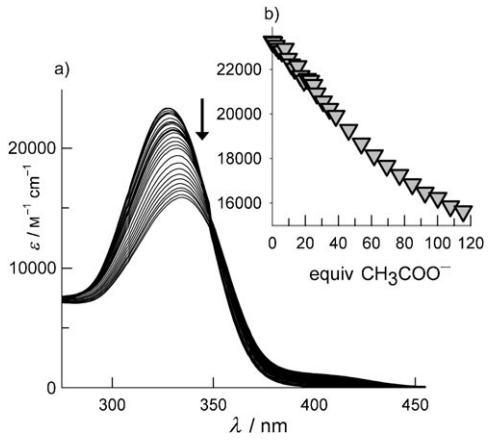

Figure 6. a) Spectra obtained over the course of the titration of a 5.00×10^{-5} M solution of **3** in $CHCl_3$ with a solution 9.62×10^{-2} M of $[Bu_4N]CH_3COO$ in $CHCl_3$; b) absorbance at 330 nm (▼).

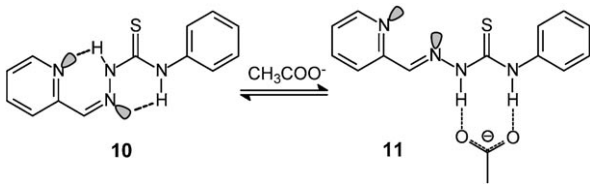

Scheme 4. Intramolecular hydrogen bonding interactions stabilize the conformation of receptor illustrated by formula **10**, which disfavours the association with oxoanions (e.g., acetate, to form complex **11**).

lar, a $\log K = 2.74\pm0.01$ was calculated from multiwavelength least-squares treatment of titration data. The development of a new band at higher wavelength was not observed even on addition of 20 equiv and more of F^-, ruling out the deprotonation of one of the N-H fragments of the thiourea subunit. It is therefore confirmed that proton release from thiourea (and urea) subunits in non-aqueous media is driven both by the high stability of the $[HF_2]^-$ self-complex and by the presence of powerful electron withdrawing substituents, in particular $-NO_2$. Receptor **5** formed a poorly stable H-bond complex also with CH_3COO^- ($\log K = 2.7\pm0.1$), as obtained from a spectrophotometric titration experiment. On titration of **5** with all the other investigated anions, no significant spectral modifications were observed, indicating the formation of association complexes of very low stability or no formation at all.

Studies on thiourea derivatives **4** and **5** have provided firm bases, which may be useful for the investigation of the anion binding tendencies of **3** (LH) and of its metal complexes $[M^{II}(LH)_2]^{2+}$ (M = Fe, Ni).

The interaction of 3 with anions and metal cations: Anion-binding tendencies of **3** towards anions in $CHCl_3$ are poor or nil. Figure 6a shows the family of spectra recorded over the course of the titration of a solution 5.00×10^{-5} M in **3** with a rather concentrated solution of $[Bu_4N]CH_3COO$ (0.1 M).

Minor spectral modifications are observed on acetate addition (up to 120 equiv). In particular, a very slight curvature is observed in the titration profile shown in Figure 6b, indicating a binding constant value $\log K \approx 1$. Less pronounced or no spectral modifications at all were observed on titration of **3** with other anions. Semiempirical investigations have shown that the uncomplexed receptor **3**, in absence of anions, exists in the conformation illustrated in Scheme 4 by formula **10**. Such an arrangement is stabilised by the presence of intramolecular hydrogen-bonding interactions involving the N-H fragments of the thiourea moiety and pyridine and imine nitrogen atoms, as outlined in Scheme 4. It is suggested that the endothermic contribution associated to the breaking of such intramolecular interactions is responsible for the poor stability of complex **11** and analogues.

Most interestingly, **3** (LH) behaves as a terdentate ligand and forms with divalent transition metals six-coordinate complexes of formula $[M^{II}(LH)_2]^{2+}$. In particular, on diffusion of diethyl ether on a MeCN solution containing $[Fe^{II}(CF_3SO_3)_2]$ and 2 equiv of **3**, violet crystals of the complex salt of formula $[Fe^{II}(LH)_2](CF_3SO_3)_2\cdot H_2O$ suitable for X-ray diffraction studies were obtained. An ORTEP view of the complex salt is shown in Figure 7.

The Fe^{II} complex exhibits a distorted octahedral coordination, with the two ligands arranged according to a meridianal coordination. Selected geometrical features are shown in Table S1 of Supporting Information.

No structures of bis(thiosemicarbazone) Fe^{II} complexes have been previously reported. However, the short Fe–N bond lengths, lying in the range 1.88(2)–1.97(2) Å, are typical for low-spin Fe^{II} octahedral complexes with ligands containing sp^2 nitrogen atoms. In particular, the Fe^{II}–N(pyridine) mean distance (1.97(1) Å) is the same as observed in the classical complexes $[Fe^{II}(bpy)_3]^{2+}$ (1.97 Å, bpy = 2,2′-bipyridine).[15] The Fe^{II}–N(imine) mean distance appears as especially short, 1.89(1) Å, if compared, for in-

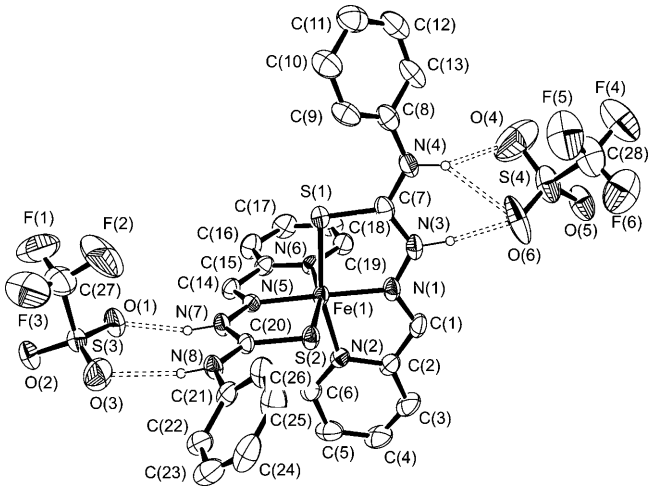

Figure 7. ORTEP view of the $[Fe^{II}(\mathbf{3})_2](CF_3SO_3)_2{\cdot}H_2O$ molecular complex (ellipsoids are drawn at the 30% probability level; the water molecule was omitted for clarity, as were hydrogen atoms not belonging to thiourea groups).

stance, with the complex $[Fe^{II}(N,N'$-dimethylethylenediimine$)_3]^{2+}$: 1.95 Å.[16] It is suggested that the unusually short Fe^{II}–N distance is a consequence of the steric constraints associated to the coordination of the terdentate ligand. The sulphur atoms are placed 2.28(1) and 2.30(1) Å from the metal centre. Such distances are distinctly lower than observed in the octahedral $[Fe^{II}(N,N'$-dimethylthiourea$)_6]^{2+}$, which has a high-spin nature and Fe^{II}–S bond lengths range over the interval 2.49–2.61 Å.[17] The two *mer*-terdentate ligands are placed in an almost perpendicular setting and the dihedral angle between the two thiosemicarbazone moieties is 89.8(4).

Very interestingly, with respect to the anion-recognition properties of the complex, each thiourea subunit establishes a bifurcate hydrogen-bonding interaction with a triflate ion. Selected features of the hydrogen-bonding interactions are shown in Table 2. Donor···acceptor distances are those observed for moderate-to-weak interactions.[18]

Notwithstanding the presence of a different solvent molecule in the crystals, MeCN instead of H_2O, the $[Ni^{II}(\mathbf{3})_2](CF_3SO_3)_2{\cdot}$MeCN complex salt is isostructural with the $[Fe^{II}(\mathbf{3})_2](CF_3SO_3)_2{\cdot}H_2O$ analogue. An ORTEP view of the complex salt is shown in Figure 8.

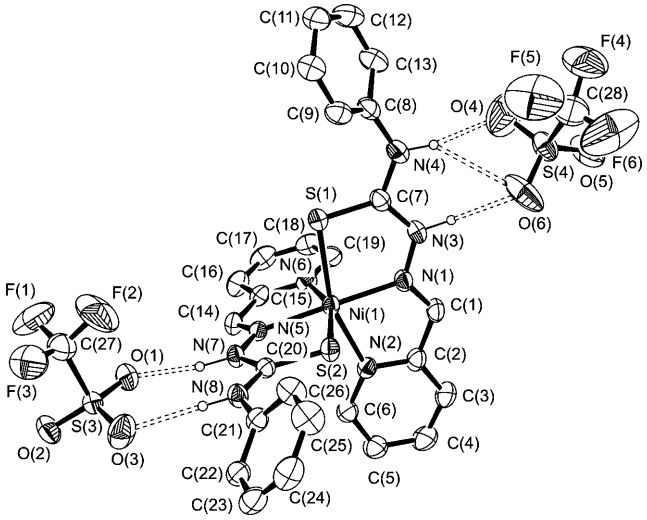

Figure 8. ORTEP view of the $[Ni^{II}(\mathbf{3})_2](CF_3SO_3)_2{\cdot}$MeCN molecular complex (ellipsoids are drawn at the 30% probability level; the MeCN molecule was omitted for clarity, as were hydrogen atoms not belonging to thiourea groups). Hydrogen bonds are drawn as dashed lines.

Actually, relevant geometrical features are similar for both compounds, as shown by values in Tables 1 and 2. Metal–donor atom distances of the Ni^{II} complex are larger than for Fe^{II}, due to the closed shell electronic configuration (t_{2g}^6) of the latter metal centre (see δ values in Table 1). Geometrical features and distances are similar to those observed in previously investigated Ni^{II} bis(thiosemicarbazones) complexes.[19,20] Also in the present case, an unusually short metal–N(imine) distance is observed, which is again ascribed to the constraints associated to the terdentate coordination mode of each thiosemicarbazone ligand (mean Ni^{II}–N(imine) = 2.01(1) Å; compare with 2.11 Å in the complex $[Ni^{II}(\text{acetaldoxime})_4Cl_2]^{2+}$,[21] or 2.10 Å in the complex $[Ni^{II}(\text{pyrazole})_6]^{2+}$).[22] Finally, structural features of the bifurcate hydrogen interactions of the two thiourea subunits are totally analogous to those of the Fe^{II} complexes, as shown by structural parameters in Table 2. Moreover, the perpendicular setting of the two *mer*-terdentate moieties, with a dihedral angle 89.3(2)°, is totally similar to that observed for the Fe^{II} analogue.

The $[Fe^{II}(LH)_2]^{2+}$ metal complex as an anion receptor: Structural studies have demonstrated that octahedral metal complexes of **3** (=HL) expose their thiourea subunits towards the outside and are therefore inclined to establish hydrogen

Table 2. Features of the hydrogen bonds involving the thiourea subunits of **3** and the triflate counterions in Fe^{II} and Ni^{II} complexes.

Donor N-H fragment		D···A [Å]	H···A [Å]	D-H···A [°]	Acceptor atom
N(3)–H(3N)	Fe^{II}	2.81(4)	1.9(2)	168(17)	O(6)
	Ni^{II}	3.00(1)	2.2(1)	145(3)	
N(4)–H(4N)	Fe^{II}	3.21(4)	2.4(2)	145(20)	O(6)
	Ni^{II}	3.38(1)	2.6(1)	138(3)	
N(4)–H(4N)	Fe^{II}	3.24(7)	2.4(3)	144(20)	O(4)
	Ni^{II}	3.06(1)	2.1(1)	164(3)	
N(7)–H(7N)	Fe^{II}	2.84(3)	1.9(2)	157(15)	O(1)
	Ni^{II}	2.83(1)	1.9(1)	172(3)	
N(8)–H(8N)	Fe^{II}	2.95(4)	2.1(2)	147(12)	O(3)
	Ni^{II}	2.99(1)	2.1(1)	161(2)	

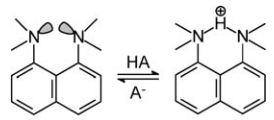

12

Scheme 5. Neutralization of a monoprotic acid HA by the Proton Sponge.

bonding interactions with anions, without experiencing any preliminary endothermic conformational rearrangement (as the uncomplexed thiosemicarbazone receptor does). Our first interest was to determine the intrinsic tendencies of thiourea N-H fragments to release protons and to characterize the deprotonated species that form, if any. Thus, we carried out a preliminary titration experiment on a $CHCl_3$ solution of the $[Fe^{II}(LH)_2]^{2+}$ complex with the Proton Sponge (**12**, N^1,N^1,N^8,N^8-tetramethylnaphthalene-1,8-diamine, Scheme 5).

Compound **12** guarantees the highest proton affinity in non-aqueous media and is not hygroscopic (like, for instance, the strong base currently used in such circumstances, $[Bu_4N]OH$). Figure 9 shows the family of spectra recorded over the course of the titration of a $CHCl_3$ solution 9.74×10^{-5} M in $[Fe^{II}(\mathbf{3})_2]^{2+}$ with a solution of **12** (1.03×10^{-2} M). In particular, Figure 9a shows the UV portion of the spectrum, displaying the ligand-to-metal charge transfer (LMCT) band; Figure 9b shows the visible part of the spectrum, with metal-to-ligand charge transfer (MLCT) bands.

On addition of base, drastic colour changes and spectral modifications are observed. Colour changes are shown in Figure S3 in the Supporting Information. The $[Fe^{II}(LH)_2]^{2+}$ complex has a violet colour, which originates from rather intense MLCT transitions. In particular, the band results from two transitions: one centred at 510 nm, the other centred at 570 nm. MLCT bands in this spectral portion are usually observed in Fe^{II} (d^6, low-spin) octahedral complexes with ligand containing sp^2 hybridized nitrogen atoms (polypyridines, imines), and result from the transitions from metal centred π orbitals (π_M, t_{2g} in origin) to π* orbitals, essentially centred on the ligands. In particular, the model 1:3 complex of Fe^{II} with the pyridine-imine ligand N-phenyl-pyridine-2-yleneamine shows a similar two-transition MLCT spectrum, with one band centred at 495 nm (shoulder, $\varepsilon=2100\,M^{-1}\,cm^{-1}$) and the other centred at 535 nm ($\varepsilon=2630\,M^{-1}\,cm^{-1}$, see Figure S4, Supporting Information). Base addition induces a dramatic red shift of the two-transition band of the $[Fe^{II}(LH)_2]^{2+}$ complex. However, the change does not take place gradually, but discontinuously. In particular, on addition of the first equivalent of base, the MLCT band of the $[Fe^{II}(LH)_2]^{2+}$ complex (solid line in Figure 9b, responsible for the violet colour) decreases in intensity, while a new band forms and develops, featuring two transitions at 535 and 607 nm (while a dark blue colour appears, see Figure S3 in the Supporting Information). On addition of the second equivalent of base, such a two-transition band decreases and a new one develops at higher wavelengths (568 and 643 nm). Such a band reaches a limiting value after the addition of 2 equiv of base, while the solution takes an emerald green colour. This behaviour can be accounted for by assuming the occurrence of the two stepwise acid–base Equilibria (3) and (4):

$$[Fe^{II}(LH)_2]^{2+} + PS \rightleftharpoons [Fe^{II}(LH)(L)]^{+} + PSH^{+} \quad (3)$$

$$[Fe^{II}(LH)(L)]^{+} + PS \rightleftharpoons [Fe^{II}(L)] + PSH^{+} \quad (4)$$

In particular, it is suggested that each proton is released from an N-H fragment of the thiourea moiety of each coordinated thiosemicarbazone. Moreover, the electron pair left on the thiourea nitrogen atom on deprotonation, formula **14**, is transferred onto the entire ligand framework, according to the π-conjugative mechanism illustrated in Scheme 6.

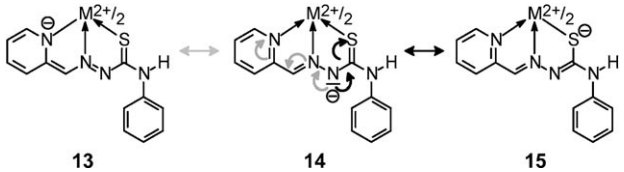

13 14 15

Scheme 6. Resonance formulae of the monodeprotonated complex $[Fe^{II}(LH)(L)]^{+}$. The lone pair left on the thiourea nitrogen atom, following N-H deprotonation, delocalizes both on the pyridine nitrogen atom (grey arrows) and on the sulphur atom (black arrows), even if to a different extent.

In particular, electron charge can be relocated onto the sulphur atom, according to the pathway illustrated by black

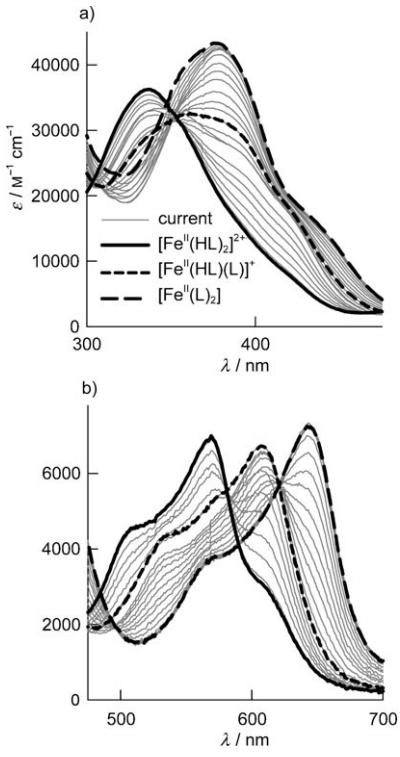

Figure 9. Spectra obtained over the course of the titration of a 9.74×10^{-5} M solution of $[Fe^{II}(\mathbf{3})_2]^{2+}$ in $CHCl_3$ with a solution 1.03×10^{-2} M of **12** in $CHCl_3$ (LH = **3**). a) UV portion, displaying LMCT bands; b) visible portion, showing MLCT bands. Thick lines refer to spectra taken after the addition of 0, 1, 2 equiv of base.

arrows in Scheme 6 (to give formula **15**) or on the pyridine nitrogen atom, according to the pathway illustrated by grey arrows (to give formula **13**). In any case, negative charge is eventually transferred from the donor atoms to the metal centre, the reducing tendencies of which increase. As a consequence, the charge transfer transition from the metal to the empty π^* orbitals centred on the pyridine–imine system becomes easier and pertinent MLCT bands are red shifted. Such an effect becomes more pronounced on successive deprotonation of an N-H fragment from the other coordinated thiosemicarbazone, which brings additional charge on the metal, whose reducing properties are further enhanced. Notice that in Scheme 6 it has been assumed that N-H deprotonation induces a simultaneous conformational change, leading to a *trans* arrangement of the phenyl substituent with respect to the sulphur atom. Such an arrangement has been observed in the 1:1 complex of Cu^{II} with a deprotonated thiosemicarbazone.[23] This would imply that the *cis* conformation, observed for instance in the $[Fe^{II}(\mathbf{3})_2](CF_3SO_3)_2$ in the solid state, is intrinsically unstable and is adopted only in the presence of hydrogen bonding bifurcate interactions of the thiourea subunit with an oxoanion (e.g., $CF_3SO_3^-$).

Figure 10 shows the profiles of the lower energy component of the MLCT band for the three species at equilibrium, $[Fe^{II}(LH)_2]^{2+}$, $[Fe^{II}(LH)(L)]^{+}$, $[Fe^{II}(L)_2]$.

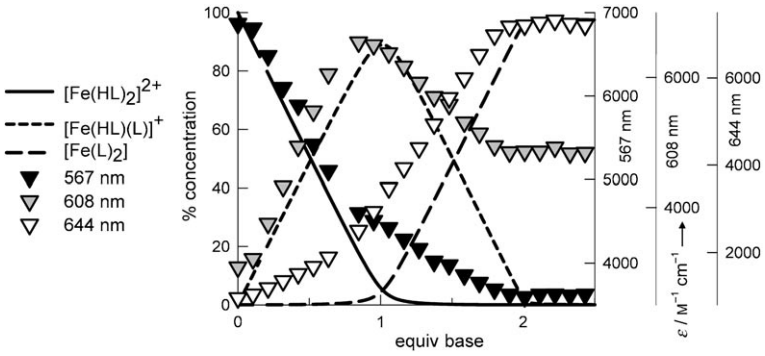

Figure 10. Symbols (ε, right vertical axes): titration profiles of the lower energy MLCT band ($\pi_M \rightarrow \pi$-pyridine) for the three species at equilibrium, $[Fe^{II}(LH)_2]^{2+}$, $[Fe^{II}(LH)(L)]^{+}$, $[Fe^{II}(L)_2]$. Lines (left vertical axis): % concentration of the three complex species calculated on assuming for equilibria (3) and (4) the following values: $\log K(3) = 13.5$, $\log K(4) = 10.0$.

The profiles show discontinuity approximately at 1 and 2 equiv of added base. Solid and dashed lines in Figure 10 represent the concentration of the $[Fe^{II}(LH)_2]^{2+}$, $[Fe^{II}(LH)(L)]^{+}$, $[Fe^{II}(L)_2]$ complexes over the course of the titration, which have been calculated on assuming for Equilibria (3) and (4) the following values: $\log K(3) = 13.5$, $\log K(4) = 10.0$. It is observed that symbols (i.e., absorbances of the low energy charge transfer bands) superimpose, at least partially, on the concentration curves. Poorly satisfactory fitting may depend on the fact that each absorbance value does not pertain to a single species, but receives minor, yet significant contributions from other complexes present at the equilibrium. In any case, diagrams in Figure 10 confirm the existence of three distinct species, with a defined stoichiometry and with different spectral properties.

The $[Fe^{II}(LH)_2]^{2+}$ complex presents also a rather intense band at 335 nm (Figure 9a). Such a band results from a transition from a donor atom of the thiosemicarbazone ligand (either sulphur or nitrogen, or both) to an empty antibonding orbital centred on the metal (σ_M^*, e_g in origin). On base addition, the intensity of such a band decreases, while a new band forms and develops at 375 nm. This behaviour clearly reflects the progress of Equilibria (3) and (4) on base addition. In particular, on N-H deprotonation, negative charge is transferred onto the donor atoms, whose reducing tendencies are increased. As a consequence, the LMCT band is significantly red shifted.

Quite interestingly, appearance and modifications of LMCT and MLCT bands over the course of the titration are definitely different. Actually, looking at spectra in Figure 9, one could assume that spectral changes in the MLCT region (Figure 9b) proceed *horizontally* (as indicated by a two-step bathochromic shift of the band) and those in the LMCT region (Figure 9a) proceed *vertically* (i.e., through the simultaneous decrease-increase of two bands). The apparently paradoxical behaviour results from the fact that the three degrees of deprotonation (0, −1, −2) generate three distinct states of charge of the metal, which give rise to three different metal-to-ligand transitions and to three limiting MLCT spectra (Figure 9b: solid, short dashed and long dashed thick lines). On the other hand, the thiosemicarbazone donor atoms (either sulphur or pyridine nitrogen atom, or both) can exist only in *two* states: either neutral or negatively charged, to which two ligand-to-metal transitions correspond: this results in two bands, one decreasing, the other increasing (Figure 9a). Thus, the intermediate species $[Fe^{II}(LH)(L)]^{+}$ does not show its specific LMCT band, but a spectrum which results from the balanced combination of the band originating from the neutral donor atom-to-Fe^{II} charge transfer and of that originating from the negatively charged donor atom-to-Fe^{II} transition.

The Brønsted acidic tendencies of $[Fe^{II}(\mathbf{3})_2]^{2+}$ in $CHCl_3$ being defined, titration experiments with anions were carried out. Figure 11 displays the family of spectra obtained over the course of the titration of a 9.74×10^{-5} M solution of $[Fe^{II}(\mathbf{3})_2]^{2+}$ in $CHCl_3$ with a solution 8.03×10^{-3} M of $[Bu_4N]CH_3COO$ in $CHCl_3$ (LH = **3**).

Quite surprisingly, on acetate addition, the same spectral pattern was obtained, as observed on titration with the

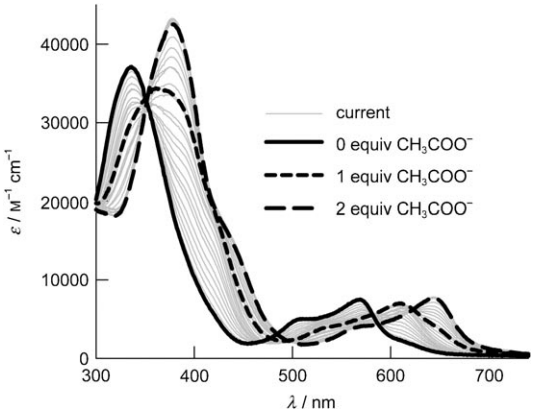

Figure 11. Spectra obtained over the course of the titration of a 9.74×10^{-5} M solution of $[Fe^{II}(\mathbf{3})_2]^{2+}$ in $CHCl_3$ with a solution 8.03×10^{-3} M of $Bu_4N]CH_3COO$ in $CHCl_3$ (LH = **3**). Thick lines refer to spectra taken after the addition of 0 (——), 1 (-----), 2 equiv (– – –) of acetate.

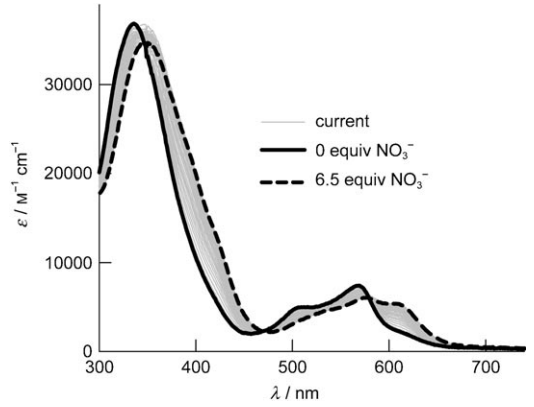

Figure 12. Spectra taken over the course of the titration of a 9.74×10^{-5} M solution of $[Fe^{II}(\mathbf{3})_2]^{2+}$ in $CHCl_3$ with a solution 1.01×10^{-2} M of $[Bu_4N]NO_3$ in $CHCl_3$ (LH = **3**). Thick lines refer to spectra taken after the addition of 0 (——) and 6.5 equiv (-----) of nitrate.

Proton Sponge. This indicates that the following stepwise acid–base equilibria take place ($X^- = CH_3COO^-$):

$$[Fe^{II}(LH)_2]^{2+} + X^- \rightleftharpoons [Fe^{II}(LH)(L)]^+ + HX \quad (5)$$

$$[Fe^{II}(LH)(L)]^+ + X^- \rightleftharpoons [Fe^{II}(L)_2] + HX \quad (6)$$

Thus, the investigated iron(II) complex appears as an extremely strong acid in $CHCl_3$, which affords definitive proton transfer from thiourea N-H fragments of the two coordinated thiosemicarbazones to the base CH_3COO^-. Strong acidity reflects the stabilization experienced by the metal complex on N-H deprotonation, due to the electron-pair delocalization towards the donor atoms and to the establishing of especially intense metal–ligand interactions. Titration experiments with $H_2PO_4^-$ and HSO_4^- induced precipitation. On titration with NO_2^-, the same spectral pattern obtained with PS and CH_3COO^- was observed (see Figure S5, Supporting Information), indicating the occurrence of acid–base Equilibria of type (5) and (6). A similar behaviour was obtained on titration with fluoride (Figure S6). Quite interestingly, each deprotonation step proceeded in presence of only 1 equiv of F^-, thus obeying to Equations (5) and (6): the diprotic acid $[Fe^{II}(\mathbf{3})_2]^{2+}$ is so strong that its stepwise deprotonation needs not to be associated to the formation of HF_2^-.

Among the investigated anions, NO_3^- exhibits a peculiar behaviour. Figure 12 shows the spectra taken over the course of the titration of a 9.74×10^{-5} M solution of $[Fe^{II}(\mathbf{3})_2]^{2+}$ in $CHCl_3$ with a solution 1.01×10^{-3} M of $[Bu_4N]$-NO_3 in $CHCl_3$. The spectral pattern is remarkably different from that observed with CH_3COO^- and involving stepwise double deprotonation: i) LMCT region: the band centred at 335 nm on nitrate addition undergoes a less pronounced red shift (from 335 to 350 nm, to be compared to 335-to-375 nm, observed with CH_3COO^-, NO_2^- and PS); moreover, on NO_3^- addition, the intensity of the band decreases; ii) MLCT region: also the two-transition MLCT band undergoes a less pronounced red shift and decreases in intensity; moreover, a continuous shift is observed, which seems to exclude the formation of two species with a different degree of deprotonation. On these bases, it is suggested that the NO_3^- establishes hydrogen-bonding interactions with the thiourea subunit of the metal coordinated thiosemicarbazone, as observed in the solid state with the $CF_3SO_3^-$ anion. In particular, the interaction should take place at the two thiourea moieties of the $[Fe^{II}(LH)_2]^{2+}$ complex, according to the stepwise Equilibria (7) and (8):

$$[Fe^{II}(LH)_2]^{2+} + NO_3^- \rightleftharpoons [Fe^{II}(LH)_2 \cdots NO_3]^+ \quad (7)$$

$$[Fe^{II}(LH)_2 \cdots NO_3]^+ + NO_3^- \rightleftharpoons [Fe^{II}(LH)_2 \cdots (NO_3)_2] \quad (8)$$

On non-linear least-squares treatment of spectrophotometric titration data over the 200–800 nm spectral range, the following stepwise constants were obtained, associated to the binding of the first [$\log K_1 = 4.78 \pm 0.06$, Eq. (7)] and of the second NO_3^- ion [$\log K_2 = 4.3 \pm 0.1$), Eq. (8)].

Figure 13 displays the concentration profiles of the species present at the equilibrium along the titration experiment. The absorbance at 615 nm (pertinent to the lower energy transition of the MLCT band of the limiting spectrum, dashed line in Figure 13) is also reported (open triangles). The latter profile does not show any discontinuity, but smoothly proceeds towards saturation. The above evidences indicate that, following the hydrogen-bonding interaction of the NO_3^- ion at the N-H fragments of the thiourea subunit, partial negative charge is transferred on the sulphur atom, which accounts for the red shift of the LMCT band. Such an effect is remarkably less pronounced than observed on deprotonation of the N-H fragment, which justifies the moderate magnitude of the red shift. Consequent transfer of negative charge on the Fe^{II} centre induces a red shift also of the MLCT band. Such a transfer of electron charge on the

metal takes place progressively, following the interaction of the first and the second NO_3^- ion with thiourea moieties. As a consequence, the red shift of the MLCT band is gradual and smooth, as shown in Figure 13, and does not show the discontinuous behaviour observed with deprotonation. Noticeably, the association of the two NO_3^- ions proceeds independently, without any mutual electrostatic or electronic influence. In particular, the difference between $\log K_1$ and $\log K_2$ (0.5 ± 0.1)) has to be ascribed to the sole statistical effect ($\approx \log 4 = 0.602$).

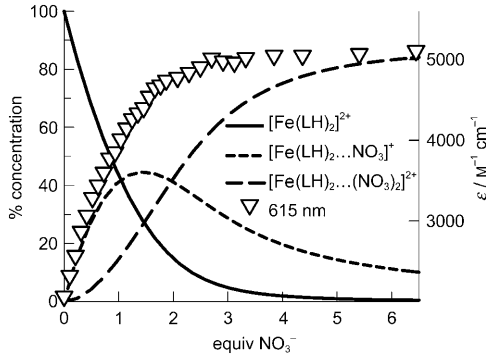

Figure 13. Lines (left vertical axis): % concentration of the three complex species: $[Fe^{II}(LH)_2]^{2+}$, $[Fe^{II}(LH)_2\cdots NO_3]^+$ and $[Fe^{II}(LH)_2\cdots(NO_3)_2]$, which form according to Equilibria (7) and (8), over the course of the spectrophotometric titration illustrated in Figure 12. Symbol (ε, right vertical axis): titration profile based on the band developing at 615 nm (lower energy of the MLCT transition pertinent to the two H-bond complexes $[Fe^{II}(LH)_2\cdots NO_3]^+$ and $[Fe^{II}(LH)_2\cdots(NO_3)_2]$).

The $[Ni^{II}(LH)_2]^{2+}$ metal complex as an anion receptor: The solution behaviour of the $[Ni^{II}(LH)_2]^{2+}$ complex is similar to that observed with the $[Fe^{II}(LH)_2]^{2+}$ analogue, with respect to both deprotonation of N-H fragments and formation of genuine hydrogen-bonding complexes.

Figure 14a shows the family of spectra recorded over the course of the titration of a solution 1.08×10^{-4} M in $[Ni^{II}(\mathbf{3})_2]^{2+}$ in $CHCl_3$ with a solution of base **12** (1.03×10^{-2} M). The spectrum of the $[Ni^{II}(\mathbf{3})_2]^{2+}$ complex, prior of base addition (thick solid line in Figure 14a), shows a rather intense band centred at 340 nm, of LMCT nature. On addition of the Proton Sponge, the LMCT band undergoes a pronounced red shift and discloses two well distinct transitions, one centred at 385 nm, the other at about 425 nm (shoulder). The titration profile, based on the band at 385 nm and displayed in Figure 14b, increases steeply and reaches a plateau on addition of 2 equiv of base. A flex is observed at 1 equiv addition. Such a spectral pattern can be accounted for on assuming the occurrence of the two stepwise deprotonation Equilibria (9) and (10), in analogy with what observed for the corresponding Fe^{II} complex:

$$[Ni^{II}(LH)_2]^{2+} + PS \rightleftharpoons [Ni^{II}(LH)(L)]^+ + PSH^+ \quad (9)$$

$$[Ni^{II}(LH)(L)]^+ + PS \rightleftharpoons [Ni^{II}(L)] + PSH^+ \quad (10)$$

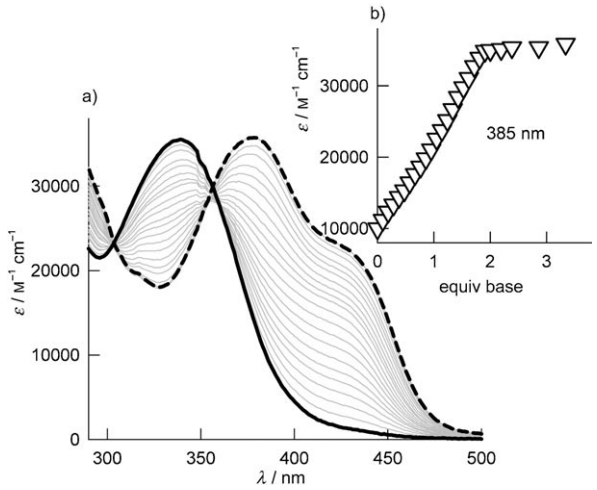

Figure 14. a) spectra recorded over the course of the titration of a 1.08×10^{-4} M solution of $[NI^{II}(LH)_2]^{2+}$ in $CHCl_3$ with a solution 1.03×10^{-2} M of **12** in $CHCl_3$ (LH = **3**); b): titration profile at 385 nm.

The nature of the spectral modifications observed during the titration has to be explained. In fact, the $[Ni^{II}(LH)_2]^{2+}$ complex shows a single band (thick solid line in Figure 14a), whereas, on stepwise deprotonation, two distinctly separated components are observed (limiting spectrum as thick dashed line in Figure 14a). We suggest that the rather broad single band of the $[Ni^{II}(LH)_2]^{2+}$ complex is the envelope of two close ligand-to-metal transitions: one from the pyridine nitrogen atom, the other from the thiourea sulphur atom. On deprotonation of the N-H fragment, charge is transferred onto the pyridine nitrogen atom and onto the sulphur atom, according to the π-delocalization mechanisms outlined in Scheme 6. However, such a charge transfer is not equally distributed over the two donor atoms. In particular, one donor atom should receive a substantially larger amount of negative charge, being thus responsible for the LMCT transition at higher wavelength. It is suggested that such a donor atom is the sulphur one and that the S-to-Fe^{II} LMCT transition is that undergoing the most pronounced red-shift. Such a hypothesis is based on structural considerations. Unfortunately, we were not able to grow crystals of the $[Ni^{II}(L)_2]$ and $[Fe^{II}(L)_2]$ complex salts suitable for X-ray diffraction studies and no structural data are available in the literature for complexes of Ni^{II} and Fe^{II} with analogous deprotonated thiosemicarbazones. However, the crystal and molecular structure has been reported for the 1:1 Cu^{II} complex of the deprotonated form of the derivative 2-Benzoylpyridine N^4-phenylthiosemicarbazone: $[Cu^{II}(L)NCS]^+$.[23] In this complex, the Cu^{II}–S distance (2.23 Å) is distinctly shorter than that observed in Cu^{II} complexes with a coordinated thiourea (e.g., $[Cu^{II}(bpy)_2(thiourea)]^{2+}$ = 2.37 Å), indicating a stronger coordinative interaction. Moreover, the C–S distance (1.75 Å) is slightly, still detectably longer than that observed in Cu^{II}-coordinated thiourea (1.72 Å), which indicates a decrease of the bond order of C=S, due to the π-delocalization pathway outlined in Scheme 6. On the other hand, no signif-

icant difference has been observed for the Cu^{II}–N(pyridine) distances in the $[Cu^{II}(L)Cl]^+$ complex (2.01 Å) and for the model compound $[Cu^{II}(pyridine)_2(H_2O)_2]^{2+}$ (2.00 Å).[24] All evidence points towards a partial thiolate nature of the coordinated sulphur atom in deprotonated thiosemicarbazones and accounts for the separation of the two LMCT transitions, as observed in the $[Ni^{II}(LH)(L)]^+$ and $[Ni^{II}(L)_2]$ complexes.

No MLCT bands are expected for a d^8 octahedral complex. This explains the less vivid colour change observed on base addition to a $CHCl_3$ solution of the $[Ni^{II}(LH)_2]^{2+}$, as compared with the $[Fe^{II}(LH)_2]^{2+}$ analogue. In particular, addition of the Proton Sponge and stepwise deprotonation caused a continuous colour variation from yellow to brown, as illustrated in Figure S7 in the Supporting Information.

On titration with CH_3COO^-, NO_2^- and F^-, the same spectral pattern was obtained, which indicated the occurrence of the stepwise acid–base Equilibria (11) and (12):

$$[Ni^{II}(LH)_2]^{2+} + X^- \rightleftharpoons [Ni^{II}(LH)(L)]^+ + HX \quad (11)$$

$$[Ni^{II}(LH)(L)]^+ + X^- \rightleftharpoons [Ni^{II}(L)] + HX \quad (12)$$

As an example, Figure 15a shows the family of spectra taken over the course of the titration of a $CHCl_3$ solution 1.35×10^{-4} M in $[Ni^{II}(\mathbf{3})_2]^{2+}$ in $CHCl_3$ with a solution of base $[Bu_4N]F\cdot3H_2O$ (1.58×10^{-2} M).

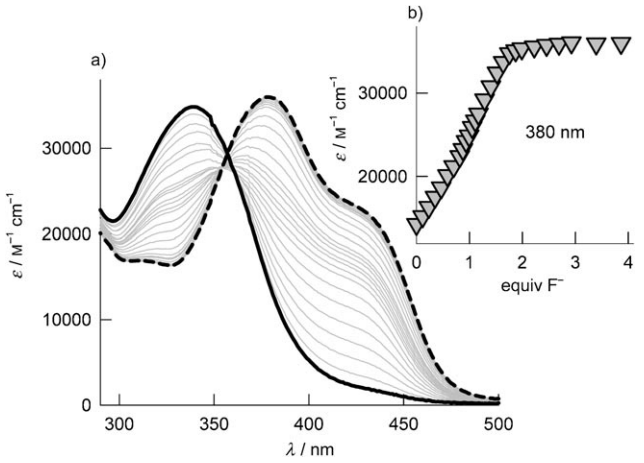

Figure 15. a) spectra obtained over the course of the titration of a 1.35×10^{-4} M solution of $[Ni^{II}(LH)_2]^{2+}$ in $CHCl_3$ with a solution 1.58×10^{-2} M of $[Bu_4N]F\cdot3H_2O$ in $CHCl_3$ (LH = **3**); b): titration profile at 380 nm.

Again, only in the case of the NO_3^- anion, the formation of authentic hydrogen bonding complexes was observed. In particular, only a moderate shift of the LMCT band was observed (see Figure 16).

Best fitting of titration data was obtained on assuming the occurrence of the stepwise Equilibria (13) and (14), to which the following association constants correspond: $\log K_1 = 5.17 \pm 0.05$, $\log K_2 = 4.3 \pm 0.1$. The difference between $\log K_1$ and $\log K_2$ slightly exceeds the statistical contribution.

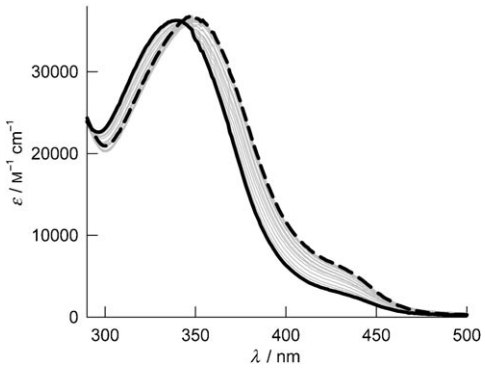

Figure 16. Spectra taken over the course of the titration of a 1.22×10^{-4} M solution of $[Ni^{II}(LH)_2]^{2+}$ in $CHCl_3$ with a solution 2.51×10^{-2} M of $[Bu_4N]NO_3$ in $CHCl_3$ (LH = **3**). Thick lines refer to spectra taken after the addition of 0 (——) and 10 equiv (-----) of nitrate.

$$[Ni^{II}(LH)_2]^{2+} + NO_3^- \rightleftharpoons [Ni^{II}(LH)_2\cdots NO_3]^+ \quad (13)$$

$$[Ni^{II}(LH)_2\cdots NO_3]^+ + NO_3^- \rightleftharpoons [Ni^{II}(LH)_2\cdots(NO_3)_2] \quad (14)$$

Figure 17 shows the concentration profiles of the species present at the equilibrium along the titration experiment illustrated in Figure 16. The absorbance at 375 nm (triangles in Figure 17) shows a continuous profile, which reaches saturation on addition of a slight excess of nitrate. In particular, absorbance values seem to result from the weighted contributions of the absorbance of the hydrogen bonding complexes at the equilibrium, $[Ni^{II}(LH)_2\cdots NO_3]^+$ and $[Ni^{II}(LH)_2\cdot\cdot(NO_3)_2]$. The moderate transfer of negative charge on the donor atoms following the H-bond interaction accounts for the moderate red shift of the LMCT band.

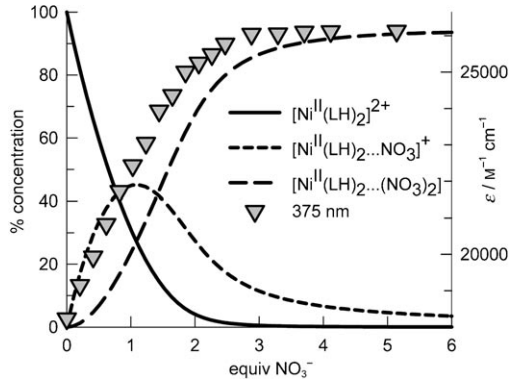

Figure 17. Lines (left vertical axis): % concentration of the three complex species $[Ni^{II}(LH)_2]^{2+}$ $[Ni^{II}(LH)_2\cdots NO_3]^+$ $[Ni^{II}(LH)_2\cdots(NO_3)_2]$, which form according to Equilibria (13) and (14), over the course of the spectrophotometric titration experiment illustrated in Figure 16. Symbol (ε right vertical axis): titration profile based on the developing LMCT band.

On titration with $[Bu_4N]H_2PO_4$ and with $[Bu_4N]HSO_4$, precipitation was observed. Even large excess addition of $[Bu_4N]ClO_4$ and $[Bu_4N]PF_6$ did not induce any significant spectral modification.

Conclusion

The intensity of hydrogen bond is related to the acidity of the donor (in anion coordination chemistry: the N-H containing receptor) and to the basicity of the acceptor (the anion): the higher receptor's acidity and anion's basicity, the stronger the hydrogen-bonding interaction and the higher the association constant. For these reasons, on one side, receptors are often equipped with electron-withdrawing substituents (i.e., the $-NO_2$ subunit) in order to improve their anion binding tendencies and, on the other side, in the absence of designed geometrical constraints, binding tendencies parallel the basic properties of the anion: $CH_3COO^- > H_2PO_4^- > HSO_4^- \approx NO_2^- > NO_3^-$. In the presence of either a strong acid or a strong base, or both, the partial and frozen proton transfer proceeds to a complete extent, with receptor's deprotonation and formation of the conjugate acid of the anion. This work has demonstrated that coordinative interaction of a 3d metal centre with the sulphur atom of the thiourea moiety of a thiosemicarbazone derivative induces an extremely high polarization of the N-H fragment, which undergoes deprotonation in presence of most anions, even if not especially basic. Such an effect had been observed, to a moderate extent, on coordination of the thiourea sulphur atom to an Ag^I centre in a scorpionate complex.[25]

Finally, it has to be noted that, upon irradiation at $\lambda >$ 300 nm, the thione form of thiourea (**a** in Scheme 7) can be converted to the tautomeric thiol form **b**, through a proton tunnelling mechanism, characterised by a high energy barrier (108 kJ mol^{-1}).[26] The thione⇄thiol tautomeric conversion could take place, in principle, through the classical deprotonation–protonation pathway illustrated in Scheme 7, a process which is prevented by the low Brønsted acidity of the thione form. This work has demonstrated that such an acidity can be highly enhanced through the sulphur coordination to a 3d divalent metal centre.

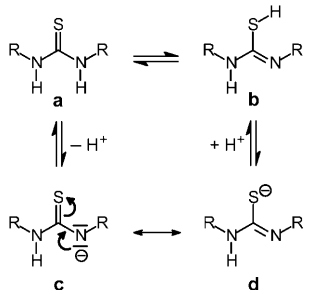

Scheme 7. Thione-to-thiol tautomeric conversion of urea derivatives.

Experimental Section

General procedures and materials: All reagents for syntheses were purchased from Aldrich/Fluka and used without further purification. All reactions were performed under N_2. UV/Vis spectra were recorded on a Varian CARY 100 spectrophotometer, with quartz cuvettes of the appropriate path length (1 or 0.1 cm). In any case, the concentration of the chromophore and the optical pathway were adjusted to obtain spectra with AU $\leq$ 1. In the titrations with anions, the UV/Vis spectra of the samples were recorded after the addition of aliquots of the tetraalkylammonium salt solution of the envisaged anion. All spectrophotometric titration curves were fitted with the HYPERQUAD program.[14] ^{1}H NMR spectra were obtained on a Bruker Avance 400 spectrometer (400 MHz) operating at 9.37 T. Mass spectra were acquired by using a Thermo-Finnigan ion-trap LCQ Advantage MAX instrument equipped with an ESI source.

Synthesis of ligand 3 (2-formylpyridine 4-thiosemicarbazone): 4-Phenylthiosemicarbazide (1.67 g, 9.98 mmol) was dissolved in methanol (50 mL) under vigorous stirring. As the solid was completely dissolved, a methanol solution of pyridine-2-carboxaldehyde (956 μL, 9.99 mmol in 30 mL) was added dropwise. A white precipitate formed after 2 h and the reaction mixture was left under stirring at room temperature for 24 h.

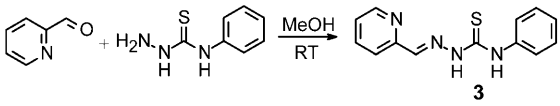

3

The mixture was filtered under vacuum and the solid was washed with several portions of cold methanol. The solid was dried under vacuum to yield **3** (2.16 g, 8.43 mmol, 90%) as a white, fibrous product. ^{1}H NMR (400 MHz, [D$_6$]DMSO): δ = 7.20 (t, ^3J(H,H) = 7.4 Hz, 1H), 7.45 (m, ^3J(H,H) = 7.9 Hz, 2H + 1H), 7.53 (d, ^3J(H,H) = 7.9 Hz, 2H), 7.81 (t, ^3J(H,H) = 7.4 Hz, 1H), 8.18 (s, 1H, imine), 8.40 (d, ^3J(H,H) = 7.9 Hz, 1H), 8.56 (d, ^3J(H,H) = 5.0 Hz, 1H), 10.35 (brs, 1H; thioureic N-H), 12.08 ppm (brs, 1H; hydrazone N-H); ESI-MS: *m*/*z* (+): 257.2 $[M+H]^+$ (100), 512.9 $[2M+H]^+$ (10); *m*/*z* (−): 255.3 $[M-H]^-$ (42), 291.2 $[M+Cl]^-$ (24), 301.1 $[M+HCOO]^-$ (100).

Synthesis of $[Fe^{II}(3)_2](CF_3SO_3)_2 \cdot H_2O$: $Fe(CF_3SO_3)_2$ (55.6 mg, 0.16 mmol) was added to a suspension of **3** (80.4 mg, 0.31 mmol) in MeCN (50 mL) in an N_2 atmosphere and under vigorous stirring. The reaction mixture, greenish in colour, was refluxed under a positive pressure of argon for 30 min, and allowed to cool to room temperature. The purple, limpid solution was concentrated in vacuo to 15 mL. Diethyl ether (100 mL) was added and the resulting solution was left to stand overnight under inert atmosphere. Precipitation occurred overnight to give a dark purple crystalline solid, which was filtered in vacuo, rapidly washed with small portions of diethyl ether, then dried in vacuo (112.3 mg, 0.13 mmol, 84%). Single crystals suitable for X-ray structural determination were chosen from this product. ^{1}H NMR (400 MHz, CD_3CN): δ = 7.28 (t, ^3J(H,H) = 7.2 Hz, 2H), 7.39 (m, ^3J(H,H) = 7.8 Hz, 4H + 2H), 7.46 (d, ^3J(H,H) = 7.8 Hz, 4H), 7.80 (t, ^3J(H,H) = 7.2 Hz, 2H), 7.93 (d, ^3J(H,H) = 6.0 Hz, 2H), 8.05 (d, ^3J(H,H) = 7.2 Hz, 2H), 9.50 (s, 2H, imine), 9.8–10.0 (brs, 2H, thioureic N-H); 12.9–13.5 ppm (brs, 2H, hydrazone N-H).

Synthesis of $[Ni^{II}(3)_2](CF_3SO_3)_2 \cdot MeCN$: $Ni(CF_3SO_3)_2$ (274.3 mg, 0.77 mmol) was added to a suspension of **3** (398.8 mg, 1.56 mmol) in MeCN (50 mL) in an N_2 atmosphere and under vigorous stirring. The pale yellow mixture was refluxed until complete dissolution (15 min), and allowed to cool down to room temperature. The dark-yellow solution was concentrated under vacuum to a final volume of 10 mL. Diethyl ether (60 mL) was then added and the resulting solution was left overnight at room temperature. A microcrystalline, brownish-yellow solid was obtained. The product was filtered under vacuum and washed with small portions of diethyl ether, then desiccated in vacuo until constant weight (485.1 mg, 0.56 mmol, 73%). Single crystals suitable for X-ray diffraction analysis were obtained by slow vapour diffusion of diethyl ether on a MeCN solution of the complex salt.

Syntheses of model compounds 4 and 5

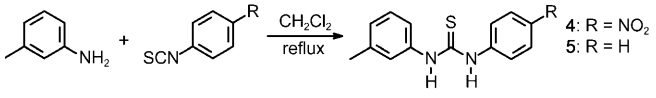

1-(4-Nitrophenyl)-3-(3-methylphenyl)thiourea (4): *m*-Toluidine (1400 μL, 12.9 mmol) was dissolved in anhydrous dichloromethane (70 mL). 4-Nitrophenylisothiocyanate (2.33 g, 12.9 mmol) was then added. The solution was refluxed for 2 h. The clear solution was allowed to cool to room temperature, to give a supersaturated solution which gave abundant precipitate after sonication. The bright yellow precipitate was filtered off by suction and the solid was washed to the analytical grade with several, small portions of cold diethyl ether, then dried under vacuum, to give a pale yellow powder (2.76 g, 9.6 mmol, 74%). ^{1}H NMR (400 MHz, $CDCl_3$): δ = 2.37 (s, 3H, benzylic), 7.14 (s, 1H), 7.15 (d, ^3J(H,H) = 6.6 Hz, 1H), 7.21 (d, ^3J(H,H) = 8.0 Hz, 1H), 7.39 (t, ^3J(H,H) = 8.0 Hz, 1H), 7.75 (d, ^3J-(H,H) = 8.8 Hz, 2H), 7.87 (brs, 1H, *N(3)*-H), 8.16 (brs, 1H, *N(1)*-H), 8.22 ppm (d, ^3J(H,H) = 8.8 Hz, 2H); ESI-MS: *m/z* (−): 159.0 [(2*M*−H)+MeOH]$^{2-}$ (45), 286.3 [*M*−H]$^-$ (58), 322.0 [*M*+Cl]$^-$ (18), 331.8 [*M*+HCOO]$^-$ (60), 400.0 [*M*+CF_3COO]$^-$ (74), 572.9 [2*M*-H]$^-$ (100), 609.0 [2*M*+Cl]$^-$ (42), 636.1 [2*M*+NO_3]$^-$ (15), 686.8 [2*M*+CF_3COO]$^-$ (34).

1-(3-Methylphenyl)-3-phenylthiourea (5): *m*-Toluidine (764 μL, 5.64 mmol) was dissolved in anhydrous dichloromethane (30 mL) under vigorous stirring. Phenylisothiocyanate (606 μL, 5.65 mmol) was rapidly added to the solution. The resulting solution was refluxed for 2 h. Then, the solution was allowed to cool to room temperature and left to stand for further 12 h. The solvent was removed with a rotary evaporator to give a pale yellow oil. After trituration with diisopropyl ether, a precipitate was obtained and filtered by suction, followed by washings with small portions of cold diisopropyl ether. The solid was then dried in vacuum to afford an ivory-coloured powder (1.190 g, 4.91 mmol, 87%). ^{1}H NMR (400 MHz, $CDCl_3$): δ = 2.34 (s, 3H, benzylic), 7.12 (d, ^3J(H,H) = 8.1 Hz, 1H), 7.19 (s, 1H), 7.21 (d, ^3J(H,H) = 8.1 Hz, 1H), 7.32 (t, ^3J-(H,H) = 7.7 Hz, 1H), 7.39–7.44 (m, 5H), 7.77 ppm (brs, 2H, thioureic N-H); ESI-MS: *m/z* (−): 241.3 [*M*-H]$^-$ (10), 277.2 [*M*+Cl]$^-$ (20), 287.0 [*M*+HCOO]$^-$ (100), 304.1 [*M*+NO_3]$^-$ (5), 354.9 [*M*+CF_3COO]$^-$ (45).

X-ray crystallographic study: Diffraction data for [Fe^{II}(**3**)$_2$]-(CF_3SO_3)$_2$·H_2O crystal have been collected at ambient temperature by means of an Enraf-Nonius CAD4 four circle diffractometer, working with graphite-monochromatized MoKα X-radiation (λ = 0.7107 Å). Data reductions (including intensity integration, background, Lorentz and polarization corrections) were performed with the WinGX package.[27] Absorption effects were evaluated with the psi-scan method[28] and absorption correction was applied to the data (min/max transmission factors were 0.748/0.851).

Diffraction data for [Ni^{II}(**3**)$_2$](CF_3SO_3)$_2$·MeCN crystal have been collected at ambient temperature by means of a Bruker-Axs CCD-based three circle diffractometer, working with graphite-monochromatized $Mo_{K\alpha}$ X-radiation (λ = 0.7107 Å). Crystals of the Ni^{II} complex were unstable under ambient conditions and data collection has been performed with the crystal placed in a closed glass capillary containing also a bit amount of mother liquor. Frames collected by the CCD based system were processed with the SAINT software[29] and intensities were corrected for Lorentz and polarization effects; absorption effects were empirically evaluated by the SADABS software[30] and absorption correction was applied to the data (0.612 and 0.848 were min and max transmission factors). Crystal data for studied crystals are shown in Table 3.

Both crystal structures were solved by direct methods (SIR 97)[30] and refined by full-matrix least-square procedures on F^2 using all reflections (SHELXL 97).[31] Anisotropic displacement parameters were refined for all non-hydrogen atoms, excluding the water oxygen of the Fe^{II} complex. Hydrogens bonded to carbon atoms were placed at calculated positions with the appropriate AFIX instructions and refined using a riding model; hydrogen bonded to the N atoms were located in the ΔF map and refined restraining the N–H distance to be 0.96 ± 0.01 Å.

CCDC 685928, 685929 contain the supplementary crystallographic data for this paper. These data can be obtained free of charge from The Cambridge Crystallographic Data Centre via www.ccdc.cam.ac.uk/data_request/cif.

Table 3. Crystal data for both iron(II) and nickel(II) complexes.

	[Fe^{II}(**3**)$_2$](CF_3SO_3)$_2$·H_2O	[Ni^{II}(**3**)$_2$](CF_3SO_3)$_2$·MeCN
formula	$C_{28}H_{26}F_6FeN_8O_7S_4$	$C_{30}H_{27}F_6N_9NiO_6S_4$
M	884.70	910.58
colour	dark red	pale red
dimensions [mm]	0.38 × 0.30 × 0.22	0.80 × 0.60 × 0.20
crystal system	triclinic	triclinic
space group	$P\bar{1}$ (no. 2)	$P\bar{1}$ (no. 2)
a [Å]	9.100(2)	9.345 (4)
b [Å]	11.393(3)	11.624(5)
c [Å]	18.563(4)	18.692(7)
α [°]	80.02(2)	77.67(1)
β [°]	83.40(2)	86.40(1)
γ [°]	75.18(2)	75.82(1)
V [Å^3]	1827.3(8)	1923.1(14)
Z	2	2
ρ_{calcd} [g cm^{-3}]	1.608	1.572
μ $Mo_{K\alpha}$ [mm^{-1}]	0.728	0.805
scan type	ω scans	ω scans
θ range [°]	1.1–25.1	1.1–25.2
measured reflns	6934	24062
unique reflns	6488	6890
R_{int}	0.032	0.025
strong data [$I_0 > 2\sigma(I_O)$]	3423	5399
refined parameters	495	518
*R*1, *wR*2 (strong data)	0.0702, 0.1712	0.0444, 0.1195
*R*1, *wR*2 (all data)	0.1505, 0.2148	0.0600, 0.1317
GOF	1.016	1.039
max/min residuals [e Å^{-3}]	1.16/−0.59	0.51/−0.37

Acknowledgements

The financial support of the Italian Ministry of University and Research (PRIN-Dispositivi Supramolecolari; FIRB-Project RBNE019H9K) is gratefully acknowledged.

[1] J. L. Sessler, P. A. Gale, W.-S. Cho, *Anion Receptor Chemistry*, Royal Society of Chemistry, Cambridge (UK), **2006**; V. Amendola, D. Esteban-Gómez, L. Fabbrizzi, M. Licchelli, *Acc. Chem. Res.* **2006**, *39*, 343; P. A. Gale, *Acc. Chem. Res.* **2006**, *39*, 465; F. P. Schmidtchen, *Coord. Chem. Rev.* **2006**, *250*, 2918; V. Amendola, M. Bonizzoni, D. Esteban-Gómez, L. Fabbrizzi, M. Licchelli, F. Sancenón, A. Taglietti, *Coord. Chem. Rev.* **2006**, *250*, 1451; A. P. Davis, *Coord. Chem. Rev.* **2006**, *250*, 2939; K. Bowman-James, *Acc. Chem. Res.* **2005**, *38*, 671; R. Martínez-Máòez, F. Sancenón, *Chem. Rev.* **2003**, *103*, 4419; P. D. Beer, P. A. Gale, *Angew. Chem.* **2001**, *113*, 502; *Angew. Chem. Int. Ed.* **2001**, *40*, 486; P. D. Beer, E. J. Hayes, *Coord. Chem. Rev.* **2003**, *240*, 167; L. Fabbrizzi, M. Licchelli, A. Taglietti, *Dalton Trans.* **2003**, 3471.

[2] K. Choi, A. D. Hamilton, *J. Am. Chem. Soc.* **2003**, *125*, 10241; S. O. Kang, J. M. Llinares, D. Powell, D. VanderVelde, K. Bowman-James, *J. Am. Chem. Soc.* **2003**, *125*, 10152; S. Otto, S. Kubik, *J. Am. Chem. Soc.* **2003**, *125*, 7804; C. R. Bondy, S. J. Loeb, *Coord. Chem. Rev.* **2003**, *240*, 77.

[3] M. A. Hossain, S. O. Kang, J. M. Llinares, D. Powell, K. Bowman-James, *Inorg. Chem.* **2003**, *42*, 5043; Y. Inoue, T. Kanbara, T. Yamamoto, *Tetrahedron Lett.* **2003**, *44*, 5167.

[4] a) J. W. Steed, *Chem. Commun.* **2006**, 2637–2649; S. L. Tobey, E. V. Anslyn, *J. Am. Chem. Soc.* **2003**, *125*, 10963; b) P. Morehouse, M. A. Hossain, J. M. Llinares, D. Powell, K. Bowman-James, *Inorg. Chem.* **2003**, *42*, 8131.

[5] P. Anzenbacher, R. Nishiyabu, M. A. Palacios, *Coord. Chem. Rev.* **2006**, 2929; J. L. Sessler, E. Katayev, G. D. Pantos, P. Scherbakov, M. D. Reshetova, V. Khrustalev, V. M. Lynch, Y. A. Ustynyuk, *J. Am. Chem. Soc.* **2005**, *127*, 11442; J. L. Sessler, J. M. Davis, *Acc. Chem. Res.* **2001**, *34*, 989.
[6] P. A. Gale, "Amide and urea based anion receptors" in *Encyclopedia of Supramolecular Chemistry*, Marcel Dekker, New York **2004**, pp. 31–41; S. Nishizawa, P. Buhlmann, M. Iwao, Y. Umezawa, *Tetrahedron Lett.* **1995**, *36*, 6483; S. Nishizawa, R. Kato, T. Hayashita, N. Teramae, *Anal. Sci.* **1998**, *14*, 595; K. P. Xiao, P. Buhlmann, Y. Umezawa, *Anal. Chem.* **1999**, *71*, 1183; J. L. J. Blanco, J. M. Benito, C. O. Mellet, J. M. G. Fernández, *Org. Lett.* **1999**, *1*, 1217; T. Hayashita, T. Onodera, R. Kato, S. Nishizawa, N. Teramae, *Chem. Commun.* **2000**, 755; T. Tozawa, Y. Misawa, S. Tokita, Y. Kubo, *Tetrahedron Lett.* **2000**, *41*, 5219; R. Kato, S. Nishizawa, T. Hayashita, N. Teramae, *Tetrahedron Lett.* **2001**, *42*, 5053; T. Gunnlaugsson, A. P. Davis, M. Glynn, *Chem. Commun.* **2001**, 2556; S. Sasaki, D. Citterio, S. Ozawa, K. Suzuki, *J. Chem. Soc. Perkin Trans. 2* **2001**, 2309; D. H. Lee, H. Y. Lee, K. H. Lee, J. L. Hong, *Chem. Commun.* **2001**, 1188; G. Hennrich, H. Sonnenschein, U. Resch-Genger, *Tetrahedron Lett.* **2001**, *42*, 2805; D. Jiménez, R. Martínez-Máñez, F. Sancenón, J. Soto, *Tetrahedron Lett.* **2002**, *43*, 2823; D. H. Lee, H. Y. Lee, J.-I. Hong, *Tetrahedron Lett.* **2002**, *43*, 7273; S. Kondo, M. Nagamine, Y. Yano, *Tetrahedron Lett.* **2003**, *44*, 8801; T. Gunnlaugsson, P. E. Kruger, T. C. Lee, R. Parkesh, F. M. Pfeffer, G. M. Hussey, *Tetrahedron Lett.* **2003**, *44*, 6575; F. Sansone, E. Chierici, A. Casnati, R. Ungaro, *Org. Biomol. Chem.* **2003**, *1*, 1802; T. Gunnlaugsson, A. P. Davis, G. M. Hussey, J. Tierney, M. Glynn, *Org. Biomol. Chem.* **2004**, *2*, 1856; V. Amendola, M. Boiocchi, B. Colasson, L. Fabbrizzi, *Inorg. Chem.* **2006**, *45*, 6138.
[7] T. Steiner, *Angew. Chem.* **2002**, *114*, 50; *Angew. Chem. Int. Ed.* **2002**, *41*, 48.
[8] F. G. Bordwell, *Acc. Chem. Res.* **1988**, *21*, 456.
[9] M. Boiocchi, L. Del Boca, D. Esteban-Gómez, L. Fabbrizzi, M. Licchelli, E. Monzani, *J. Am. Chem. Soc.* **2004**, *126*, 16507; D. Esteban-Gómez, L. Fabbrizzi, M. Licchelli, *J. Org. Chem.* **2005**, *70*, 5717–5720; M. Boiocchi, L. Del Boca, D. Esteban-Gómez, L. Fabbrizzi, M. Licchelli, E. Monzani, *Chem. Eur. J.* **2005**, *11*, 3097.
[10] S. Gronert, *J. Am. Chem. Soc.* **1993**, *115*, 10258.
[11] D. Esteban-Gómez, L. Fabbrizzi, M. Licchelli, E. Monzani, *Org. Biomol. Chem.* **2005**, *3*, 1495.
[12] C. Pérez-Casas, A. K. Yatsimirsky, *J. Org. Chem.* **2008**, *73*, 2275.
[13] M. Bonizzoni, L. Fabbrizzi, A. Taglietti, F. Tiengo, *Eur. J. Org. Chem.* **2006**, 3567.
[14] P. Gans, A. Sabatini, A. Vacca, *Talanta* **1996**, *43*, 1739; http://www.hyperquad.co.uk/index.htm; accessed 25 April, 2008.
[15] F. H. Allen, *Acta Crystallogr. Sect. B* **2002**, *58*, 380.
[16] M. J. Blandamer, J. Burgess, J. Fawcett, P. Guardado, C. D. Hubbard, S. Nuttall, L. J. S. Prouse, S. Radulovic, D. R. Russell, *Inorg. Chem.* **1992**, *31*, 1383.
[17] J. P. Fackler, T. Moyer, J. A. Costamagna, R. Latorre, J. Granifo, *Inorg. Chem.* **1987**, *26*, 836.
[18] G. A. Jeffrey, *An Introduction to Hydrogen Bonding*, Oxford University Press, Oxford, **1997**.
[19] N. C. Kasuga, K. Sekino, C. Koumo, N. Shimada, M. Ishikawa, K. Nomiya, *J. Inorg. Biochem.* **2001**, *84*, 55.
[20] I. Garcýa, E. Bermejo, A. K. El Sawaf, A. Castineiras, D. X. West, *Polyhedron* **2002**, *21*, 729.
[21] M. E. Stone, B. E. Robertson, E. Stanley, *J. Chem. Soc. A* **1971**, 3632.
[22] R. W. M. ten Hoedt, W. L. Driessen, G. C. Verschoor, *Acta Crystallogr. Sect. C* **1983**, *39*, 71.
[23] M. Joseph, M. Kuriakose, M. R. P. Kurup, E. Suresh, A. Kishore, S. G. Bhat, *Polyhedron* **2006**, *25*, 61.
[24] E. Cannillo, G. Giuseppetti, *Atti Accad. Naz. Lincei* **1964**, *36*, 878.
[25] V. Amendola, D. Esteban-Gómez, L. Fabbrizzi, M. Licchelli, E. Monzani, F. Sancenón, *Inorg. Chem.* **2005**, *44*, 8690.
[26] H. Rostkowska, L. Lapinski, A. Khvorostov, M. J. Nowak, *J. Phys. Chem. A* **2003**, *107*, 6373.
[27] L. J. Farrugia, *J. Appl. Crystallogr.* **1999**, *32*, 837.
[28] A. C. T. North, D. C. Phillips, F. S. Mathews, *Acta. Crystallogr. Sect. A* **1968**, *24*, 351.
[29] SAINT-NT Software Reference Manual, Version 6, Bruker AXS Inc., Madison, Wisconsin, USA, **2003**.
[30] A. Altomare, M. C. Burla, M. Camalli, G. L. Cascarano, C. Giacovazzo, A. Guagliardi, A. G. G. Moliterni, G. Polidori, R. Spagna, *J. Appl. Crystallogr.* **1999**, *32*, 115.
[31] G. M. Sheldrick, SHELX97 Programs for Crystal Structure Analysis, University of Göttingen (Germany), **1997**.

Received: April 27, 2008
Published online: September 12, 2008

